

Thermodynamic and hydrodynamic constraints on overpressure caused by hydrate dissociation: A pore-scale model

R. Holtzman¹ and R. Juanes¹

Received 28 April 2011; accepted 4 May 2011; published 21 July 2011.

[1] It has been suggested that volume expansion caused by hydrate dissociation in sediment pores can result in large overpressure, which in turn may destabilize the sediment and trigger massive submarine landslides. Here, we investigate the pressure evolution during thermally-induced dissociation, by means of a pore-scale model that couples dissociation kinetics, multiphase flow and geomechanics. Dissociation is controlled by a self-preservation mechanism: increasing pore pressure reduces the driving force for dissociation. Hence, the overpressure is constrained by the phase equilibrium pressure, regardless of the kinetic rate of dissociation, heat supply, and sediment permeability. Furthermore, we find that the timescale for buildup of pressure by dissociation is typically much larger than that for its dissipation by drainage. Consequently, the overpressure is controlled by the capillary entry thresholds, which depend on the mode of gas invasion. In low-permeability systems, fracturing is the preferred mechanism, occurring at capillary pressures lower than the entry thresholds in the undeformed sediment. Our results suggest that while large overpressures cannot be sustained by rapid dissociation in natural systems, dissociation can induce important geomechanical effects. Gas migration by fracturing provides a possible link between dissociation, sediment deformation and methane venting. **Citation:** Holtzman, R., and R. Juanes (2011), Thermodynamic and hydrodynamic constraints on overpressure caused by hydrate dissociation: A pore-scale model, *Geophys. Res. Lett.*, 38, L14308, doi:10.1029/2011GL047937.

1. Introduction

[2] Methane hydrate is a solid compound that forms by crystallization of water and methane upon cooling and/or pressurization. Accumulations of methane hydrate in hydrate-bearing sediments (HBS) have gained much attention for their potential as an energy resource [Boswell, 2009] and their role as a greenhouse gas in future global warming [Archer et al., 2009]. Heating or depressurization cause hydrate to dissociate into free gas and water. Dissociation of hydrate within the pore space of sediments has often been invoked as a mechanism that may lead to significant overpressures (up to tens of MPa), in view of the multiple-fold volume increase that occurs upon dissociation [Xu and Germanovich, 2006; Kwon et al., 2008; Rutqvist and Moridis, 2009]. Overpressure induced by dissociation has been suggested as a trigger for

sediment failure, including submarine landslides [Sultan et al., 2004; Mienert et al., 2005; Xu and Germanovich, 2006], soft-sediment deformation [Kennett and Fackler-Adams, 2000], pingo-like features [Paull et al., 2007], mud volcanoes [Van Rensbergen et al., 2002] and wellbore damage [Rutqvist and Moridis, 2009]. Warming of ocean waters and consequent dissociation of extensive HBS layers, leading to sediment failure and massive release of methane gas, has been proposed as the cause of the Paleocene-Eocene Thermal Maximum [Dickens et al., 1995], and as a potential key player in the current carbon cycle [Dickens, 2003; Westbrook et al., 2009].

[3] The possible implications of dissociation raise the need for understanding the relevant mechanisms, in particular the interplay between dissociation and pressure evolution. Existing models predict large overpressures in fine-grained sediments, where the low permeability would prevent rapid pressure dissipation [Xu and Germanovich, 2006; Kwon et al., 2008; Rutqvist and Moridis, 2009; Kwon et al., 2010]. Xu and Germanovich [2006] evaluate overpressures as high as 50 MPa for undrained (no-flow) conditions and 7 MPa for low permeability sediment, assuming a constant dissociation rate which is independent of the pore pressure. The end-member scenario of no flow and restricted volumetric expansion was investigated by Kwon et al. [2008], who correctly point out that since rising pressure stalls further dissociation, additional heat is required to continue the dissociation process. This self-preservation mechanism leads to pressure-temperature (p-T) conditions which follow the three-phase (hydrate-gas-brine) equilibrium curve during dissociation. Therefore, a large overpressure (hereafter defined as the gas pressure above the initial water pressure p_0 prior to dissociation) implies a large temperature increase; for example, an increase of ~ 9 MPa is accompanied by a temperature rise of over 9°C [Kwon et al., 2008]. A pressure increase of tens of MPa requires heating by tens of degrees. Simulating long-term thermal stimulation by a hot wellbore (90°C), Rutqvist and Moridis [2009] predict overpressures of ~ 15 MPa in nearby sediments. Smaller pressures (less than 3 MPa) were predicted by Kwon et al. [2010] in simulating dissociation due to a wellbore ($\sim 20^\circ\text{C}$ warmer than its surrounding) in a low-permeability clay. While the authors honor self-preservation by constraining the pressure by the equilibrium pressure, they do not account for dissociation kinetics, and assume that hydrate saturation is sufficiently low to neglect gas flow. However, we will show that gas flow and percolation can occur at hydrate saturations as low as 5%, in agreement with Tsimpanogiannis and Lichtner [2006].

[4] A crucial mechanism which is missing from the models cited above is the coupling among dissociation

¹Department of Civil and Environmental Engineering, Massachusetts Institute of Technology, Cambridge, Massachusetts, USA.

kinetics, flow of gas and water, and sediment deformation, including the formation of preferential flow paths and fractures. Consideration of this mechanism requires description of the pore-scale physics. *Tsimpanogiannis and Lichtner* [2006] investigated the flow patterns of methane gas produced by heating an HBS, and showed that larger pore apertures and a broader range of aperture sizes allow larger gas quantities to percolate through a sample, hence increasing the gas productivity. The authors used a pore-network model based on invasion percolation, assuming instantaneous dissociation and fixed network properties (no geomechanical effects).

[5] In this paper we study the pressure evolution during thermally-induced dissociation. We present a mechanistic, pore-scale model that couples dissociation kinetics, multiphase flow and sediment mechanics. We explore the range of behaviors between the two end-members: (a) no-flow (undrained) conditions; and (b) instantaneous pressure dissipation (fully drained). We model the physics at the pore scale and thus perform all computations at the pore level. The collective dynamics give rise to global effects such as pressurization of the entire sample and gas-invasion patterns. While upscaling the results from our simulations with millimeter-size samples to the reservoir scale is not straightforward, our model elucidates fundamental mechanisms that control the sediment behavior at the pore scale. We demonstrate that rapid pressure buildup is not possible because of the negative feedback between dissociation rate and fluid pressure. The strict upper bound for the gas pressure is its thermodynamic limit: the equilibrium pressure. However, for typical values of the kinetic rates and medium permeability, our results show that pressure buildup by dissociation is slow compared with pressure dissipation by drainage. As a result, overpressures are controlled by the value of the gas pressure required to invade into the porous medium, and are typically much lower than the equilibrium pressure.

2. Model Formulation

[6] We simulate a low-permeability sample saturated with water and dispersed hydrate crystals, subjected to a sudden temperature increase which brings hydrate out of thermodynamic equilibrium. The small inhibiting effect of the latent heat on the dissociation rate allows us to consider isothermal dissociation under fixed, uniform temperature and exclude heat transfer effects (see Text S1 of the auxiliary material).¹ We evaluate the temporal and spatial evolution of the mass, volume and pressure of hydrate, water and gas, and their impact on the sediment's mechanical and flow properties. At each time step we compute: (1) the dissociated hydrate mass for every crystal, given the surrounding fluid pressures; (2) pore pressure variations caused by the conversion of hydrate into water and gas; (3) flow of gas and water induced by the rising pore pressure; and (4) changes in hydraulic properties by deformation of the solid matrix (microstructural rearrangements). We emphasize in our model the role of multiphase flow by assuming that the driving force for the flow is the generation of pressurized gas by hydrate

dissociation. Once gas pressure overcomes the local capillary thresholds, gas expands by invading into nearby water-filled pores. We evaluate the pressure of gas clusters as they expand and coalesce and the local increase in water pressure due to fluid redistribution along the gas-water interface [*Måløy et al.*, 1992; *Xu et al.*, 2008].

[7] We capture the interplay between pore pressure and dissociation by computing the decomposition rate of each hydrate crystal using a kinetic model. The hydrate mass dissociated during each time step Δt , $\Delta m_h = (dm_h/dt) \Delta t$, is determined according to a driving force which is proportional to the difference between the phase equilibrium fugacity f_{eq} and the methane fugacity at the hydrate crystal surface f [*Kim et al.*, 1987],

$$\frac{dm_h}{dt} = -K_h \exp\left(\frac{-E}{RT}\right) F_A A_h (f_{eq} - f), \quad (1)$$

where K_h is the hydration reaction constant, E is the hydration activation energy, A_h is the surface area for the reaction, and $R = 8.314 \text{ J mol}^{-1} \text{ K}^{-1}$ is the universal gas constant. Negative Δm_h implies decreasing mass. The area A_h is computed from the hydrate crystal volume (which is updated in time as it shrinks), assuming spherical crystal with area adjustment factor of $F_A = 1$. We evaluate f_{eq} and f from the equilibrium pressure p_{eq} (for a given temperature T) and the pressure of gas surrounding the dissociating crystal, p_g . The reverse process, hydrate reformation, can occur locally upon reversal of the driving force ($p_{eq} < p_g$) [*Waite et al.*, 2008]; this process is excluded from our current model.

[8] The gas pressure in each gas cluster, p_g , is evaluated through the ideal-gas equation of state (EOS), where we compute the cluster volume V_g from mass balance. Each mole of dissociated hydrate (with volume of $\Delta V_h = M_h/\rho_h$) is converted to N_h moles of water, which occupies a volume of $\Delta V_w = N_h M_w/\rho_w$. Here, $\rho_h = 900 \text{ kg/m}^3$, $M_h = 0.119 \text{ kg/mol}$, $\rho_w = 1000 \text{ kg/m}^3$ and $M_w = 0.018 \text{ kg/mol}$ are the density and molar mass of methane hydrate and water, respectively, and $N_h = 5.75$ is the hydration number [*Sloan and Koh*, 2008]. To obtain the cluster volume V_g we note that $\Delta V_w/\Delta V_h \approx 0.8$, hence the remainder 20% of the dissociated hydrate volume ΔV_h is replaced with gas. For simplicity, we use here the ideal gas law, $p_g V_g = n_g RT$, where n_g is the number of gas moles in the cluster. We have confirmed that the use of a more accurate EOS does not alter our results substantially; for example, the difference between overpressures evaluated with the ideal gas law and with the EOS by *Duan et al.* [1992] in several representative simulations is $\sim 0.1\%$. The number of gas moles n_g is computed from the number of dissociated hydrate moles, $\Delta n_h = \Delta m_h/M_h$. Given the low solubility of methane in water [*Sloan and Koh*, 2008], we consider only two methane phases, hydrate and gas, neglecting the small quantities that dissolve in water.

[9] Our model incorporates the two-way coupling between fluid displacement and mechanical deformation: pore opening in response to pressure loading (direct coupling), and alteration of the flow properties by grain rearrangements (reverse coupling) [*Holtzman and Juanes*, 2010]. A deformable porous material is represented by a 2-D square lattice of dented blocks (grains), connected

¹Auxiliary materials are available in the HTML. doi:10.1029/2011GL047937.

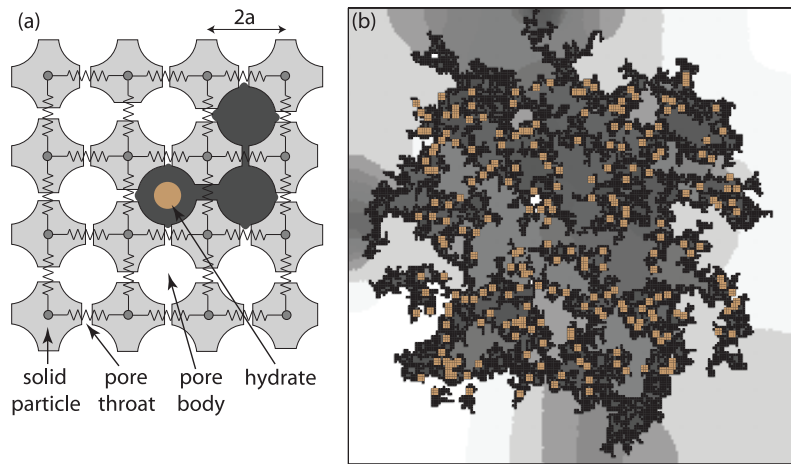


Figure 1. (a) Schematic of the pore-scale model. The solid matrix is represented by a square lattice of dented blocks (grains), connected mechanically by springs. The narrow openings between the grains are the pore throats, which connect the larger openings (pore bodies). Some pores are filled with hydrate crystals (brown), which decompose into water (white) and free gas (dark gray). (b) Pore pressure during simulation of dissociation. The grayscale intensity represents the pressure scaled to increase contrast: white corresponds to the ambient pressure p_0 , black to high pressures in gas filled pores. The location of clusters of 3×3 pores originally occupied by hydrate crystals is marked in brown. The pressure halo that develops ahead of newly invaded pores reflects the finite timescale required for pressure dissipation. We use a network of 200×200 pores with $\lambda = 0.2$, $\epsilon_0 = 0.01$, $a = 1 \mu\text{m}$, $\mu = 10^{-3} \text{ Pa s}$ and $\gamma = 0.07 \text{ N/m}$. A system in equilibrium at $T_0 = 0.5^\circ\text{C}$ and $p_0 = 2.58 \text{ MPa}$ is subjected to $\Delta T = 10^\circ\text{C}$.

mechanically by nonlinear springs (Figure 1a). The voids between the blocks define a pore network: the narrow openings at the contacts are the pore throats, which connect the larger openings (pore bodies). Variation in block shapes leads to variability in throat apertures, which is assumed to be uncorrelated in space. This provides two interacting networks, solid and fluid, whose nodes are the grain centers and the pore bodies, respectively. We solve for displacement of the grains and fluid pressures at the pore bodies.

[10] Pore-scale disorder in hydraulic properties is represented by assigning a distribution of initial area A and permeability k to the pore throats. Both parameters scale with the square of the throat aperture r , that is, $A \sim r^2$, $k \sim r^2$ (assuming Stokes flow in cylindrical tubes provides $A = \pi r^2$, $k = r^2/8$). We characterize the disorder in the hydraulic properties through a scalar parameter, $\lambda \in (0,1)$, drawing values from a uniform distribution, $r \in [1 - \lambda, 1 + \lambda]\bar{r}$, where $\bar{r} \sim a$. The characteristic length scale is the pore size a , which here we take as half the distance between nodes in the lattice (Figure 1a). Partially-drained conditions are simulated through a decrease in permeability and throat area at the boundary (each by 3 orders of magnitude, equivalent to a reduction in throat aperture by a factor of $10^{3/2}$) relative to the sample's interior. We enforce a constant hydrostatic pressure p_0 at the boundary pores.

[11] In simulating flow we assume that gas is inviscid, such that its pressure adjusts instantaneously and is uniform within each cluster. The water pressure in a water-filled pore is updated from mass conservation at a pore body: $p_w(t + \Delta t) = p_w(t) + \sum_j q^j \Delta t / (c_t V)$, where V is the pore volume, c_t is an effective compressibility of the system (see below), and the summation is over all neighboring pores. The volumetric flow rate between the pore and its neighbor j is

given by Darcy's law $q^j = (Ak/\mu)(p^j - p_w)/\ell^j$, where μ is the water dynamic viscosity and ℓ^j is the length over which the pressure drop $p^j - p_w$ occurs. For flow between two water-filled pores, $\ell^j = 2a$. If pore j is gas-filled, the meniscus between the two pores starts advancing once the capillary pressure exceeds the capillary entry pressure, $p^j - p_w > 2\gamma/r$, where γ is the gas-water interfacial tension. As the meniscus advances, the length is updated by $\ell^j(t + \Delta t) = \ell^j(t) - (q^j/A)\Delta t$.

[12] The gas generated by hydrate dissociation invades the porous medium, displacing water. Slow drainage in disordered media occurs in the form of bursts ("Haines jumps" [Haines, 1930]), which lead to sudden changes in water pressure. When one or more pores are invaded during a burst, the interface menisci at neighboring pores readjust, receding along throats or even leading to a backfilling of previously invaded pores [Måløy *et al.*, 1992; Xu *et al.*, 2008]. This phenomenon suppresses further invasion until the excess water pressure is dissipated, thus limiting the burst size. The aggregate behavior resulting from this phenomenon is an effective system compressibility, $c_t = a/\gamma$ [Holtzman and Juanes, 2010] (see Text S1 of the auxiliary material). The finite time required for pressure dissipation leads to the development of a pressure halo around the expanding gas clusters (Figure 1b; see also Animation S1 in the auxiliary material).

[13] Changes in pore pressure cause grain rearrangements, which are represented in our model through contraction of the springs over time, $h(t)$. We highlight the effect of disorder in flow properties by using uniform spring stiffness K and enforcing an initially uniform contraction of all spring, h_0 , corresponding to a macroscopic strain $\epsilon_0 = h_0/2a$. This guarantees an initially uniform pre-stressed state, which

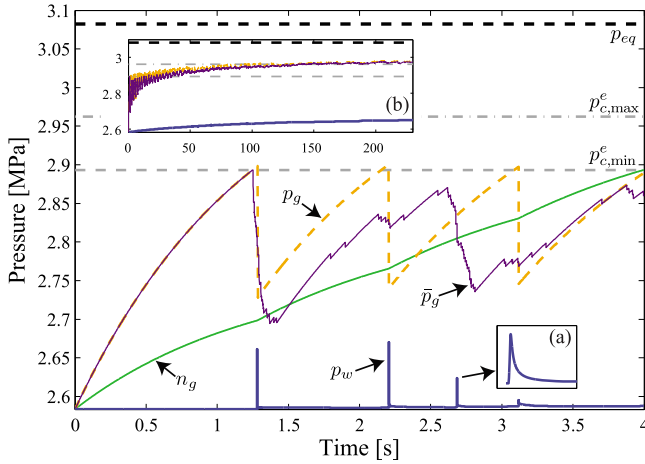


Figure 2. Pressure evolution during thermally-induced hydrate dissociation. The pressures p_g and p_w shown in the plot are measured in a specific gas cluster and in an adjacent pore, respectively. The effect of expansion and coalescence of different gas clusters is captured by the mean gas pressure, $\bar{p}_g = \sum_j (p^j V^j) / \sum_j V^j$ (summation over all gas-filled pores); see Animation S2 of the auxiliary material. The concave shape of both the gas pressure p_g and the (normalized) number of moles within a cluster n_g demonstrates the self-preservation mechanism: reduction in dissociation rate as p_g increases. The sharp drop in p_g marks gas expansion during an invasion event: once p_g exceeds the sum of the capillary entry pressure p_c^e and the water pressure in an adjacent water-filled pore p_w , gas invades that pore. The timescale for pressure buildup by dissociation, $t_d \sim 1$ s, is 5 orders of magnitude larger than that of pressure dissipation following an invasion event, $t_p \sim 10^{-5}$ s (between the peak and the plateau in inset (a)). During the entire simulation (inset (b)), the gas pressure is constrained by both thermodynamics ($p_g < p_{eq}$) and hydrodynamics ($p_g < p_c^e + p_w$). We used a network of 100×100 pores and $\lambda = 0.1$. Here, we simulated a relative low temperature increase, $\Delta T = 1.5^\circ\text{C}$, to emphasize the effect of self-preservation.

becomes spatially-variable upon hydrate dissociation. The confinement ϵ_0 is sufficiently large to prevent granular flow. Each grain is subject to two types of forces: pressure and contact forces. The force exerted by the fluid occupying an adjacent pore body is oriented at 45° relative to the lattice axes and is of magnitude $f_p = pA_p$, where $A_p \sim a^2$ is the area upon which the pressure p acts. The intergranular contact forces f_c are updated by $f_c(t + \Delta t) = f_c(t) + K\Delta h$, where $\Delta h = h(t + \Delta t) - h(t)$ is the change in spring contraction. Grain positions are determined at the new time step by imposing force balance at every grain, $\sum(\vec{f}_p + \vec{f}_c) = \vec{0}$, which leads to a linear system of equations in Δh . Grain displacements impact fluid flow by modifying the throat apertures. We evaluate changes in apertures and in intergranular forces from the grain displacements in analogy with cubic packing of spherical grains with frictionless, Hertzian contacts, such that $\Delta r = -\Delta h(1 - \epsilon) \left[2\sqrt{1 + (1 - \epsilon)^2} \right]$, where $\epsilon = h(t)/2a$

[Jain and Juanes, 2009], and $K = 2E^* \sqrt{R^*h}$, where $R^* = a/2$, and E^* is the constrained Young modulus of the grain

material [Johnson, 1987; Holtzman and Juanes, 2010]. We model an unconsolidated sediment with negligible tensile strength. Therefore, a spring is removed when there is net elongation between blocks ($h < 0$). A small cohesive force is applied as a regularization parameter.

3. Results

[14] Our simulations demonstrate that the pressure always remains below the equilibrium value, $p_{eq}(T)$. Self-preservation, where increasing gas pressure diminishes the driving force for further dissociation (equation (1)), is evident from the decreasing rate of pressure buildup by dissociation between gas invasion (pore filling) events. Furthermore, comparison of the gas and water pressure evolution indicates that the timescale for pressure buildup by dissociation, t_d , is much larger than that of pressure dissipation following gas invasion of one or more pores and water flow ahead of the moving meniscus, t_p (Figure 2). The contrast in timescales can be deduced by scaling: $t_p \sim L_p^2/D$, where $D = (k/\mu)/c_t$ is the hydraulic diffusivity, and L_p is the characteristic distance over which pressure dissipation takes place. With $k \sim a^2$ and $c_t \sim a/\gamma$ we obtain $t_p \sim \mu L_p^2/(\gamma a)$. The dissociation timescale can be obtained from equation (1), by using the EOS to relate the change in the number of gas moles ($-\Delta m_h/M_h$) to the change in gas pressure, Δp_g , and assuming that the latter scales as the fugacity driving force, $\Delta p_g \sim f_{eq} - f$. This provides $t_d \sim M_h a / [RTK_h \exp(-E/RT)]$. Using published values of $E = 8.1 \times 10^4$ J mol $^{-1}$ and $K_h = 3.6 \times 10^4$ kg m $^{-2}$ Pa $^{-1}$ s $^{-1}$ [Clark and Bishnoi, 2001] suggests that t_p is smaller than t_d by 4 to 8 orders of magnitude, depending on the value of L_p ; $L_p \sim a$ provides an upper bound of 10^8 , whereas the contrast becomes smaller as L_p approaches the system size. Since L_p reflects the spacing between gas clusters, the timescale ratio will be between the two values.

[15] The rapid dissipation of pressure by drainage relative to its buildup by dissociation implies that the pressure evolution is governed by capillary effects: once the gas pressure exceeds the sum of the water pressure p_w and entry pressure p_c^e in an adjacent water-filled pore, gas expands by invasion and its pressure drops. For the scale of interest here, we can understand gas invasion driven by hydrate dissociation as a quasi-static process, where the water pressure relaxes quickly to a value close to p_0 (Figure 2). Thus, gas overpressure is controlled by the capillary entry thresholds for gas invasion.

[16] To demonstrate the role of capillarity we compare the maximum pressure that develops during the simulations (until complete dissociation) in systems of different permeability. We vary the permeability by scaling a given aperture distribution (r_0 , similar in all samples) by a pore-to-throat parameter $\beta = r_0/r$, keeping the pore size a fixed. The resulting gas overpressures in most simulations are bounded between the minimum and maximum capillary entry pressures, $p_{c,min}^e = 2\gamma/[(1 + \lambda)\bar{r}]$ and $p_{c,max}^e = 2\gamma/[(1 - \lambda)\bar{r}]$, with values closer to $p_{c,max}^e$ as the permeability increases and to $p_{c,min}^e$ as it gets smaller (Figure 3). This behavior is caused by two mechanisms: heterogeneity and matrix deformation. The higher capillary pressures that develop in low-permeability systems result in smaller number of invaded pores (higher-density gas compressed

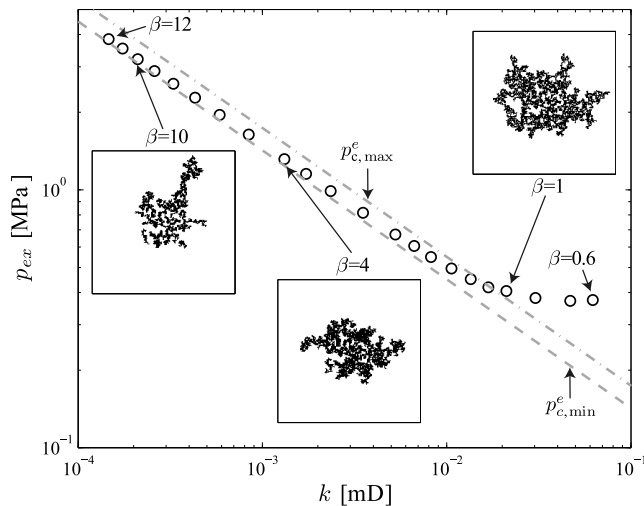


Figure 3. Mean overpressure $p_{ex} = \bar{p}_g - p_0$ and typical invasion pattern (insets) in systems of different permeability $k \sim \bar{r}^2$ (varied by scaling the aperture distribution by β). Because dissipation of pressure by drainage is much faster than its buildup by dissociation, the overpressure is governed by the capillary entry thresholds. In most simulations, $p_{c,min}^e < p_{ex} < p_{c,max}^e$. As the permeability becomes smaller, p_{ex} approaches the lower bound $p_{c,min}^e$, due to the combined effect of heterogeneity and deformation. In low-permeability systems, the highly-pressurized gas occupies a smaller volume and hence samples a smaller portion of the aperture distribution, with only the widest throats (lowest p_c^e) invaded. In addition, the high capillary pressures can lead to fracture opening, which is the preferred mode of gas invasion in soft, fine-grained sediments (see Figure 4). In the coarsest samples ($k > 0.02$ mD), the overpressures slightly exceed $p_{c,max}^e$ (by ~ 0.1 MPa) due to a similar increase in water pressure (Figure 2) which elevates the gas pressure required for invasion. Such pressure increment is negligible relative to the high gas pressure that develops in lower-permeability systems. We use networks of 100×100 and 200×200 pores for the main plot and the insets, respectively, with $\lambda = 0.1$ and $E^* = 2$ GPa.

into a smaller volume), where the invasion of only the widest throats (lowest p_c^e) implies that a smaller portion of the aperture distribution is sampled. In addition, higher capillary entry pressures cause more pore opening through grain rearrangements, creating fractures [Jain and Juanes, 2009; Holtzman and Juanes, 2010]. Fracturing allows gas invasion at a capillary pressure lower than the original threshold p_c^e in the undeformed system. Fractures as conduits for gas migration have been observed in experiments [Boudreau et al., 2005] and inferred in the field [Scandella et al., 2011]. In our model, for a given aperture distribution, the mode of invasion is determined by the grain stiffness (E^*) and the external confinement (ϵ): fracturing tends to occur in softer sediments under lower confinement [Holtzman and Juanes, 2010]. In addition, fracturing is more pronounced in sediments with lower heterogeneity in hydraulic properties, corresponding to smaller values of λ (Figure 4).

[17] Finally, the scaling of the characteristic time for dissociation t_d suggests that it can become comparable to

that of pressure dissipation t_p if the kinetics were much faster, that is, for much larger reaction constant K_h or characteristic distance L_p values. We investigate this theoretical limit by simulating dissociation with K_h values up to 10^4 higher than published values [Clark and Bishnoi, 2001]. While the resulting overpressures are higher than those of a quasi-static process controlled by the capillary entry pressures, they always remain well below the thermodynamic equilibrium value p_{eq} .

4. Conclusions

[18] In conclusion, we have shown that the overpressure from hydrate dissociation in sediments is governed by the competition between kinetic dissociation rate and pressure dissipation. Due to self-preservation, the overpressures cannot exceed the phase equilibrium pressure, regardless of the heat supply and sediment permeability. If the intrinsic kinetic rate was many orders of magnitude faster than its published value, the dissociation rate could be controlled by the ability of the medium to dissipate the pressure. Our results suggest, however, that the timescale for pressure buildup by dissociation is much larger than that of pressure dissipation by drainage, even for low-permeability sediments. We can thus view gas invasion driven by dissociation as a quasi-static process, where the water pressure relaxes quickly and the gas pressure is limited by the characteristic capillary thresholds. Hence, the pressure evolution is dominated by hydrodynamics, where the maximum pressure depends on the mode of gas invasion. In systems with large pore apertures, gas invades with negligible amount of matrix deformation, and the overpressures are constrained by the capillary thresholds. The overpressure may be further limited by geomechanical effects, especially in soft, low-permeability sediments where fracturing is the preferred gas invasion mechanism. Gas invasion by way of fracturing is a mechanism that offers a plausible explanation for massive sediment failure and methane venting by hydrate dissociation.

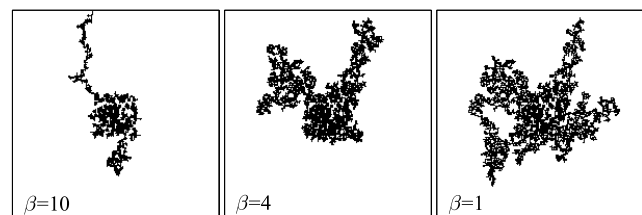


Figure 4. Modes of gas invasion following hydrate dissociation in systems of different permeability, showing a transition from capillary fingering for more permeable media ($\beta = 1$) to fracture opening for less permeable media ($\beta = 10$). In these simulations, we used parameters reflecting slightly lower pore-scale heterogeneity ($\lambda = 0.05$), slightly softer grains ($E^* = 1.85$ GPa) and more concentrated hydrate distribution at the center of the sample than in Figure 3. Hydrate dissociation in the low-permeability medium ($\beta = 10$) leads to the creation and propagation of a fracture (see Animation S3 of the auxiliary material).

[19] **Acknowledgments.** We gratefully acknowledge financial support for this work, provided by Eni S.p.A. and by the ARCO Chair in Energy Studies.

[20] The Editor thanks Hugh Daigle for his assistance in evaluating this paper.

References

- Archer, D., B. Buffett, and V. Brovkin (2009), Ocean methane hydrates as a slow tipping point in the global carbon cycle, *Proc. Natl. Acad. Sci. U. S. A.*, *106*(49), 20,596–20,601.
- Boswell, R. (2009), Is gas hydrate energy within reach?, *Science*, *325* (5943), 957–958.
- Boudreau, B. P., C. Algar, B. D. Johnson, I. Croudace, A. Reed, Y. Furukawa, K. M. Dorgan, P. A. Jumars, and A. S. Grader (2005), Bubble growth and rise in soft sediments, *Geology*, *33*(6), 517–520.
- Clark, M., and P. R. Bishnoi (2001), Determination of activation energy and intrinsic rate constant of methane gas hydrate decomposition, *Can. J. Chem. Eng.*, *79*(1), 143–147.
- Dickens, G. R. (2003), Rethinking the global carbon cycle with a large, dynamic and microbially mediated gas hydrate capacitor, *Earth Planet. Sci. Lett.*, *213*, 169–183.
- Dickens, G. R., J. R. O'Neil, D. K. Rea, and R. M. Owen (1995), Dissociation of oceanic methane hydrate as a cause of the carbon isotope excursion at the end of the Paleocene, *Paleoceanography*, *10*(6), 965–971.
- Duan, Z. H., N. Møller, and J. H. Weare (1992), An equation of state for the CH₄-CO₂-H₂O system: I. Pure systems from 0 to 1000°C and 0 to 8000 bar, *Geochim. Cosmochim. Acta*, *56*(7), 2605–2617.
- Haines, W. B. (1930), Studies in the physical properties of soils. V. The hysteresis effect in capillary properties, and the modes of moisture redistribution associated therewith, *J. Agric. Sci.*, *20*, 97–116.
- Holtzman, R., and R. Juanes (2010), Crossover from fingering to fracturing in deformable disordered media, *Phys. Rev. E*, *82*(4), 046305, doi:10.1103/PhysRevE.82.046305.
- Jain, A. K., and R. Juanes (2009), Preferential Mode of gas invasion in sediments: Grain-scale mechanistic model of coupled multiphase fluid flow and sediment mechanics, *J. Geophys. Res.*, *114*, B08101, doi:10.1029/2008JB006002.
- Johnson, K. L. (1987), *Contact Mechanics*, Cambridge Univ. Press, Cambridge, U. K.
- Kennett, J. P., and B. N. Fackler-Adams (2000), Relationship of clathrate instability to sediment deformation in the upper Neogene of California, *Geology*, *28*(3), 215–218.
- Kim, H. C., P. R. Bishnoi, R. A. Heideman, and S. S. H. Rizvi (1987), Kinetics of methane hydrate decomposition, *Chem. Eng. Sci.*, *42*(7), 1645–1653.
- Kwon, T.-H., G.-C. Cho, and J. C. Santamarina (2008), Gas hydrate dissociation in sediments: Pressure-temperature evolution, *Geochem. Geophys. Geosyst.*, *9*, Q03019, doi:10.1029/2007GC001920.
- Kwon, T.-H., K.-I. Song, and G.-C. Cho (2010), Destabilization of marine gas hydrate-bearing sediments induced by a hot wellbore: A numerical approach, *Energy Fuels*, *24*(10), 5493–5507.
- Måløy, K. J., L. Furuberg, J. Feder, and T. Jøssang (1992), Dynamics of slow drainage in porous media, *Phys. Rev. Lett.*, *68*(14), 2161–2164.
- Mienert, J., M. Vanneste, S. Bünz, K. Andreassen, H. Haflidason, and H. P. ejrup (2005), Ocean warming and gas hydrate stability on the mid-Norwegian margin at the Storegga slide, *Mar. Pet. Geol.*, *22*(1–2), 233–244.
- Paull, C. K., W. Ussler III, S. R. Dallimore, S. M. Blasco, T. D. Lorenson, H. Melling, B. E. Medioli, F. M. Nixon, and F. A. McLaughlin (2007), Origin of pingo-like features on the Beaufort Sea shelf and their possible relationship to decomposing methane gas hydrates, *Geophys. Res. Lett.*, *34*, L01603, doi:10.1029/2006GL027977.
- Rutqvist, J., and G. J. Moridis (2009), Numerical studies on the geomechanical stability of hydrate-bearing sediments, *SPE J.*, *14*(2), 267–282.
- Scandella, B. P., C. Varadharajan, H. F. Hemond, C. Ruppel, and R. Juanes (2011), A conduit dilation model of methane venting from lake sediments, *Geophys. Res. Lett.*, *38*, L06408, doi:10.1029/2011GL046768.
- Sloan, E. D., and C. A. Koh (2008), *Clathrate Hydrates of Natural Gases*, 3rd ed., CRC Press, Boca Raton, Fla.
- Sultan, N., P. Cochonat, J.-P. Foucher, and J. Mienert (2004), Effect of gas hydrates melting on seafloor slope instability, *Mar. Geol.*, *213*, 379–401.
- Tsimpanogiannis, I. N., and P. C. Lichtner (2006), Pore-network study of methane hydrate dissociation, *Phys. Rev. E*, *74*(5), 056303, doi:10.1103/PhysRevE.74.056303.
- Van Rensbergen, P., M. De Batist, J. Klerkx, R. Hus, J. Poort, M. Vanneste, N. Granin, O. Khlystov, and P. Krinitsky (2002), Sublacustrine mud volcanoes and methane seeps caused by dissociation of gas hydrates in Lake Baikal, *Geology*, *30*(7), 631–634.
- Waite, W. F., T. J. Kneafsey, W. J. Winters, and D. H. Mason (2008), Physical property changes in hydrate-bearing sediment due to depressurization and subsequent repressurization, *J. Geophys. Res.*, *113*, B07102, doi:10.1029/2007JB005351.
- Westbrook, G. K., et al. (2009), Escape of methane gas from the seabed along the West Spitsbergen continental margin, *Geophys. Res. Lett.*, *36*, L15608, doi:10.1029/2009GL039191.
- Xu, L., S. Davies, A. B. Schofield, and D. A. Weitz (2008), Dynamics of drying in 3D porous media, *Phys. Rev. Lett.*, *101*, 094502, doi:10.1103/PhysRevLett.101.094502.
- Xu, W., and L. N. Germanovich (2006), Excess pore pressure resulting from methane hydrate dissociation in marine sediments: A theoretical approach, *J. Geophys. Res.*, *111*, B01104, doi:10.1029/2004JB003600.

R. Holtzman and R. Juanes, Department of Civil and Environmental Engineering, Massachusetts Institute of Technology, Bldg. 48, 77 Massachusetts Ave., Cambridge, MA 02139, USA. (rholtzman@mit.edu; juanes@mit.edu)